Rayleigh wave constraints on the structure and tectonic history of the Gamburtsev Subglacial Mountains, East Antarctica

David S. Heeszel,[1,2] Douglas A. Wiens,[1] Andrew A. Nyblade,[3] Samantha E. Hansen,[4] Masaki Kanao,[5] Meijan An,[6] and Yue Zhao[6]

Received 13 December 2012; revised 21 March 2013; accepted 25 March 2013; published 10 May 2013.

[1] The Gamburtsev Subglacial Mountains (GSM), located near the center of East Antarctica, remain one of the most enigmatic mountain ranges on Earth. A lack of direct geologic samples renders their tectonic history almost totally unconstrained. We utilize teleseismic Rayleigh wave data from a 2 year deployment of broadband seismic stations across the region to image shear velocity structure and analyze the lithospheric age of the GSM and surrounding regions. We solve for 2-D phase velocities and invert these results for 3-D shear velocity structure. We perform a Monte Carlo simulation to improve constraints of crustal thickness and shear velocity structure. Beneath the core of the GSM, we find crustal thickness in excess of 55 km. Mantle shear velocities remain faster than global average models to a depth of approximately 250 km, indicating a thick lithospheric root. Thinner crust and slower upper mantle velocities are observed beneath the Lambert Rift System and the Polar Subglacial Basin. When compared with phase velocity curves corresponding to specific tectonothermal ages elsewhere in the world, average phase velocity results for the GSM are consistent with regions of Archean-Paleoproterozoic origin. Combined with radiometric ages of detrital zircons found offshore, these results indicate a region of old crust that has undergone repeated periods of uplift and erosion, most recently during the Mesozoic breakup of Gondwana. Lower crustal seismic velocities imply a moderately dense lower crust beneath the core of the GSM, but with lower density than suggested by recent gravity models.

Citation: Heeszel, D. S., D. A. Wiens, A. A. Nyblade, S. E. Hansen, M. Kanao, M. An, and Y. Zhao (2013), Rayleigh wave constraints on the structure and tectonic history of the Gamburtsev Subglacial Mountains, East Antarctica, *J. Geophys. Res. Solid Earth*, *118*, 2138–2153, doi:10.1002/jgrb.50171.

1. Introduction

[2] The Gamburtsev Subglacial Mountains (GSM) are located near the center of the East Antarctic Ice Sheet (Figure 1). Bedrock elevations in the region exceed 2000 m [*Bo et al*., 2009; *Fretwell et al*., 2013], and the region is a proposed nucleation point for the formation of the continental ice sheet at 34 Ma [*DeConto and Pollard*, 2003a, 2003b]. Recent ground-based and airborne radar surveys have revealed significant relief within the GSM [*Bell et al*., 2011; *Bo et al*., 2009; *Ferraccioli et al*., 2011] (Figure 1). The region is defined by large mountain peaks and deeply incised fluvial/glacial valleys [*Bo et al*., 2009]. The extension of the Lambert Rift System (LRS) into the study region is evident as a large, deeply incised, system of valleys that extends into the northern portion of the study area with potential extension around the core of the GSM [*Ferraccioli et al*., 2011]. The amount of observed topographic relief and the overall pattern and structure of the valleys suggest that there has been both fluvial and glacial erosion, pointing to a relatively recent origin for modern GSM topography [*Bo et al*., 2009].

[3] Persistent questions regarding the origin of the GSM are their mechanism of uplift and age. These questions have important implications for the development of glaciers and ice sheets within central East Antarctica [*DeConto and Pollard*, 2003b]. Historically, it has often been assumed that the central region of Antarctica is composed of a single Archean aged crustal block [*Tingey*, 1991]. Recent studies have suggested a more complicated tectonic history for the

Additional supporting information may be found in the online version of this article.

[1]Department of Earth and Planetary Sciences, Washington University in St. Louis, St. Louis, Missouri, USA.
[2]Scripps Institution of Oceanography, University of California—San Diego, La Jolla, California, USA.
[3]Department of Geosciences, Pennsylvania State University, University Park, Pennsylvania, USA.
[4]Department of Geological Sciences, University of Alabama, Tuscaloosa, Alabama, USA.
[5]Geoscience Research Group and Polar Data Center, National Institute of Polar Research, Tokyo, Japan.
[6]Institute of Geomechanics, Chinese Academy of Geological Sciences, Beijing, China.

Corresponding author: D. S. Heeszel, Scripps Institution of Oceanography, University of California—San Diego, La Jolla, CA 92093, USA. (dheeszel@ucsd.edu)

2169-9313/13/10.1002/jgrb.50171

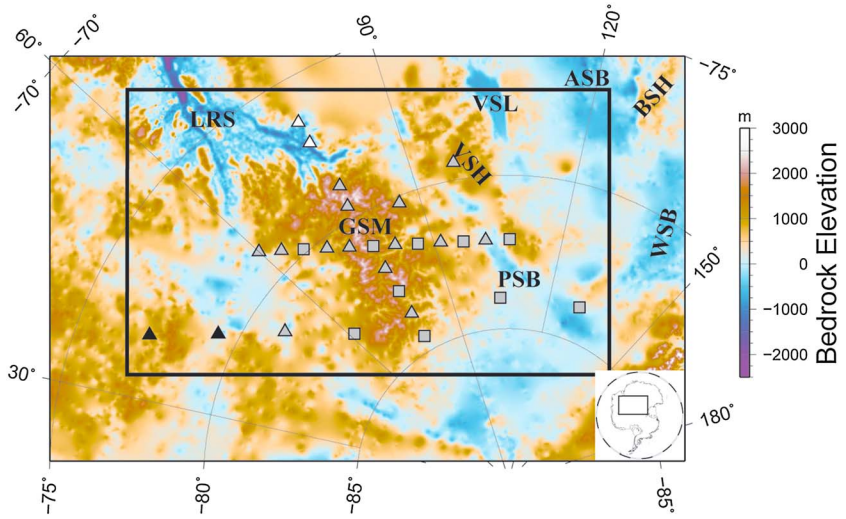

Figure 1. Subglacial bedrock topography of study region [*Fretwell et al*., 2013]. Stations in grey operated by the U.S., squares ran for 2 years, triangles for 1 year. Stations in black were operated by Japan and those in white by China (Table 1). Major topographic features labeled: GSM, Gamburtsev Subglacial Mountains; VSH, Vostok Subglacial Basin; LRS, Lambert Rift System; VSL, Vostok Subglacial Lake; ASB, Aurora Subglacial Basin; BSH, Belgica Subglacial Highlands; PSB, Polar Subglacial Basin. Heavy outline denotes region imaged in this study. (inset) Map of Antarctica with mapped region outlined in black.

region [*Boger*, 2011; *Ferraccioli et al*., 2011; *Fitzsimons*, 2003; *Studinger et al*., 2003], though the region is still believed to be composed of Archean and Proterozoic crustal blocks. The apparent disconnect between high topography and old crust has led to a number of hypotheses for the formation of the GSM. Researchers have suggested that the GSM are a thermally supported plateau [*Sleep*, 2006] or the result of far field stresses related to the formation of Pangaea during the Late Carboniferous–Early Permian [*Veevers*, 1994; *Veevers et al*., 2008a, 2008b]. A variation on this idea is a two-stage uplift in which the crust is initially thickened during the Early Permian and additional uplift is associated with Cretaceous rifting in the LRS during the breakup of Gondwana [*Ferraccioli et al*., 2011; *Lisker et al*., 2003; *Phillips and Läufer*, 2009]. Other researchers have suggested that the GSM formed during multiple Neoproterozoic–early Paleozoic orogenic events associated with the formation of Gondwana [*Fitzsimons*, 2000, 2003; *Liu et al*., 2002, 2009; *Zhao et al*., 2003]. Despite the importance of the GSM in our understanding of Antarctic tectonics, no direct observations of their geology exist due to the thick ice cover in the region (>1000 m). Recent geochronology results from an International Ocean Drilling Program site in Prydz Bay have dated detrital zircons at 529–546 Ma [*van de Flierdt et al*., 2008; *Veevers et al*., 2008a] supporting a possible Neoproterozoic or Early Paleozoic origin for the region, perhaps related to the formation of Gondwana.

[4] In addition to a lack of direct geologic evidence, comprehensive studies of the crust and upper mantle structure are also lacking for the GSM. Previous seismological investigations of the region are limited to continent-wide studies using global data sets [*Morelli and Danesi*, 2004; *Ritzwoller et al*., 2001; *Roult and Rouland*, 1992] and have lateral resolutions greater than 500 km. These studies have shown that the structure of the GSM is defined by a thick crust and a seismically fast, cratonic lithosphere. However, they have been unable to capture smaller-scale complexities within the region and so are of limited utility in constructing models of its tectonic history. Crustal thickness estimates from gravimetric and satellite data are able to provide some insight into the regions tectonic history, though estimates vary widely from ~42 to 65 km [*Block et al*., 2009; *Ferraccioli et al*., 2011; *von Frese et al*., 1999].

[5] The recent Gamburtsev Antarctic Mountain Seismic Experiment (GAMSEIS), part of the broader Antarctica's Gamburtsev Province (AGAP) IPY initiative, was a 2 year deployment of 28 broadband seismographs across the Dome A region of East Antarctica (Table 1 and Figure 1). This array provides an excellent opportunity to image the crust and upper mantle structure of the region at a resolution that has not been achievable previously. Recent receiver function analysis of the GSM using GAMSEIS data has found crustal thicknesses in excess of 55 km beneath the core of the mountain range and thicknesses of 40–45 km in surrounding regions [*Hansen et al*., 2009, 2010]. Receiver functions provide strong constraints on the existence and depth of discontinuities, such as the Moho directly beneath the seismic stations, but provide little direct constraint on the crustal and mantle shear velocities and structure in regions between stations. In this study, we utilize teleseismic Rayleigh waves at periods of 18–182 s to image the crust and upper mantle shear wave structure of the GSM region and adjacent areas of East Antarctica.

2. Data and Methods

2.1. Data Acquisition

[6] Data were collected by a temporary array of 28 broadband seismographs deployed across the GSM by the U.S., Japanese, and Chinese Antarctic programs as part of a joint IPY initiative to study the region (Table 1 and Figure 1). The array design consisted of an oblique cross consisting

Table 1. Station Names, Locations, and Operating Periods for the Gamburtsev Subglacial Mountain Seismic Experiment (GAMSEIS)

Station Name	Latitude	Longitude	Operating Nation	Operating Years
N124	−82.07	107.64	U.S.	Dec 2007 to Jan 2009
N132	−82.08	101.95	U.S.	Jan 2008 to Jan 2009
N140	−82.01	96.77	U.S.	Dec 2007 to Jan 2009
N148	−81.86	91.51	U.S.	Jan 2008 to Jan 2009
N156	−81.67	86.50	U.S.	Dec 2007 to Jan 2009
N165	−81.41	81.76	U.S.	Jan 2008 to Jan 2009
N173	−81.11	77.47	U.S.	Dec 2007 to Jan 2009
N182	−80.74	73.19	U.S.	Jan 2008 to Jan 2009
N190	−80.33	69.43	U.S.	Jan 2008 to Jan 2009
N198	−79.86	65.96	U.S.	Dec 2007 to Jan 2009
N206	−79.39	62.86	U.S.	01/2008 to 01/2009
N215	−78.90	59.99	U.S.	01/2008 to 01/2009
P061	−84.50	77.22	U.S.	12/2007 to 01/2009
P071	−83.65	77.33	U.S.	Jan 2008 to Jan 2009
P080	−82.81	77.36	U.S.	Dec 2007 to Jan 2009
P090	−81.94	77.31	U.S.	Jan 2008 to Jan 2009
P116	−79.57	77.05	U.S.	Jan 2008 to Jan 2009
P124	−78.87	77.66	U.S.	Jan 2008 to Jan 2009
GM01	−83.99	104.73	U.S.	Dec 2007 to Jan 2009
GM02	−79.43	97.58	U.S.	Jan 2008 to Jan 2009
GM03	−80.22	85.94	U.S.	Jan 2008 to Jan 2009
GM04	−83.00	61.11	U.S.	Dec 2007 to Jan 2009
GM05	−81.18	51.16	U.S.	Jan 2008 to Jan 2009
GM06	−79.33	44.31	Japan	Jan 2008 to Jan 2009
GM07	−77.31	39.61	Japan	Jan 2008 to Jan 2009
AGO1	−83.86	129.61	U.S.	Dec 2007 to Jan 2009
EGLE	−76.42	77.03	China	Summer 2007/2008 and 2008/2009
CHNB	−77.17	76.98	China	Summer 2008/2009

of 19 stations with nine outlying stations designed to improve 3-D resolution across the region. The two lines had lengths of 910 km (Stations N124–N215) and 630 km (stations P061–P124), respectively (Table 1 and Figure 1). The U.S. and Japanese stations consisted of either cold-rated Guralp CMG-3T or Nanometrics T-240 broadband sensors coupled with Quanterra Q330 digital acquisition systems with GPS timing and solid-state memory. The Chinese stations used cold-rated Guralp GMG-3T sensors with Guralp DM24 digital acquisition systems. Using a novel station design developed for polar applications by IRIS-PASSCAL, we were able to operate the U.S.-deployed stations throughout the polar night [*Johns et al.*, 2006]. Sensors were placed on insulated piers buried slightly below (~1 m) the snow surface, and station electronics were buried nearby in insulated boxes that also contained batteries. Summer power was provided by solar panels and, in some cases, wind generators connected to absorbed glass mat batteries, while winter power was provided by a bank of primary lithium batteries. A low-voltage disconnect automatically switches station power from absorbed glass mat to lithium batteries at the end of the austral summer and back when sufficient sunlight is available to reliably charge the absorbed glass mats. A heating pad that operated directly from the solar panel provided some internal heating. The station design was capable of consistently maintaining temperatures within the electronics box greater than 20°C above ambient temperature and resulted in a data recovery of ~93% for the U.S.-deployed stations.

[7] The U.S. and Japanese stations were installed using Dehavilland Twin Otter aircraft equipped with skis. Chinese stations were installed by overland traverse along the route from Zhongshan Station, on the coast, to Dome A. The U.S. deployment consisted of a pilot year (December 2007 to December 2008) of 10 stations (Figure 1) and a second year (December 2008 to December 2009) of 24. Two Japanese stations operated near Dome F were installed in late 2008, and the two Chinese stations were operated during the 2007–2008 and 2008–2009 austral summers.

2.2. Phase Velocity Inversion

[8] We utilize fundamental-mode Rayleigh wave data generated by earthquakes at epicentral distances of 30°–150° and depths of less than 100 km (Figure 2). We set a minimum surface wave magnitude (M_S) of 4.5 for earthquakes at epicentral distances between 30° and 60° and 5.5 for greater distances. We apply this dual-selection criterion to take advantage of the relatively small earthquakes at smaller epicentral distances along the circum-Antarctic ridge system. Seismograms are time-windowed around the fundamental-mode Rayleigh wave at 25 periods from 18 to 182 s. We eliminate data with signs of significant beating, low signal-to-noise ratio, or interfering phases. We use only earthquakes that produce high-quality data at more than six stations to limit uncertainty in modeling wavefront parameters [*Yang and Forsyth*, 2006].

[9] Phase velocity inversion is performed using the two-plane wave method [*Forsyth and Li*, 2005], a method that uses the phase and amplitude information from each station to model the incoming wavefield as the interference of two-plane waves. The method is better able to account for off great circle path effects, scattering, and multipathing caused by velocity heterogeneity between the source and study area when compared to traditional surface wave methods [*Forsyth and Li*, 2005; *Li et al.*, 2003]. We first perform an inversion for the average structure across the study region. This average curve is then used as a starting model for 2-D inversions at a grid of nodes across the study

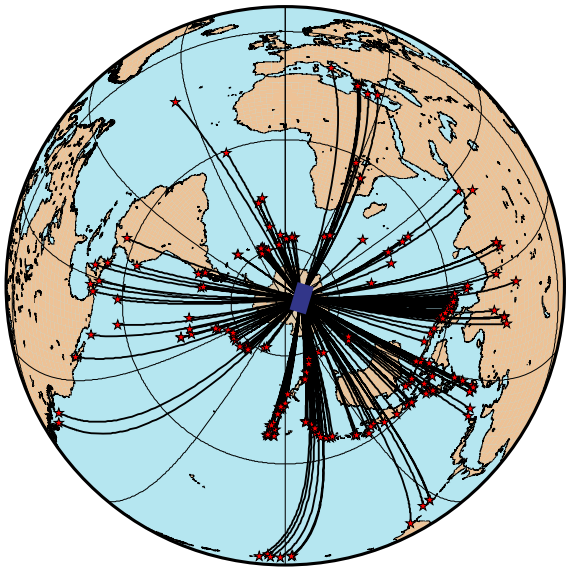

Figure 2. Azimuthal equidistant map of earthquakes (red stars) used in this study. Great circle paths to station N173 near the center of the array plotted in black, study region in dark blue. Latitude and longitude are plotted in plotted in 60° and 30° increments, respectively.

region (Figure 3). We parameterize our region into 486 nodes with a primary central region having a node spacing of 80 km and an outer region of nodes having a spacing of 160 km. The outer region of nodes is necessary to absorb the effects of misfit to the two-plane wave approximation, primarily due to wavefield scattering outside of the study region. For 2-D phase velocity inversions, we incorporate the use of finite-frequency sensitivity kernels [*Yang and Forsyth*, 2006] using the Born approximation [*Zhou et al*., 2004]. The inclusion of finite-frequency effects improves discrimination and location of off-great circle energy in the inversion scheme. Additionally, we solve for azimuthal anisotropy terms across the study region.

[10] Phase velocity is solved for continuously across the study region and discretized at the location of the nodes. Final phase velocity maps are constructed using a 2-D Gaussian weighted interpolation of the inversion results to determine the phase velocity across the region [*Forsyth and Li*, 2005]. The averaging length of the Gaussian interpolation represents a compromise between resolution and variance. To test this trade-off, we apply a variety of averaging lengths between 60 and 300 km at 20 km increments. We find that an averaging length of 100 km provides the best trade-off between resolution and variance in the period range of 18–58 s, which are the periods most sensitive to the velocity structure of the crust and uppermost mantle, and apply this averaging length throughout the period range of the study.

2.3. Shear Velocity Inversion

2.3.1. Linear Inversion

[11] We invert our phase velocity maps for a depth-dependent shear velocity structure using a two-stage approach similar to that outlined by *Ritzwoller et al*. [2001]. We first extract an average phase velocity curve at each node and invert for the shear velocity in a linear least squares sense [*Herrmann and Ammon*, 2002]. To investigate the model space around the resulting inverse model, we conduct Monte Carlo resampling of the region around the initial inverse model. These 1-D models are then interpolated using the same 2-D Gaussian smoothing operator applied to construct the phase velocity maps.

[12] An important constraint on the inversion of shallow shear velocity structure is the thickness of the ice layer. However, since we are smoothing our results over a large spatial area, uncertainties in ice thickness values of a few hundred meters are acceptable. To this end, we use ice thickness values from BEDMAP [*Lythe et al*., 2001] since it is a large, self-consistent data set that is usually consistent, to within a few hundred meters, with *P* wave receiver functions or airborne radar which are more accurate but do not extend throughout the study area [*Hansen et al*., 2010]. Initial crustal thickness estimates and average crustal velocities are based on *S* wave receiver functions [*Hansen et al*., 2010] supplemented with receiver functions of surrounding regions [*Hansen et al*., 2009; *Reading*, 2006]. We interpolate these crustal thickness estimates on the same length scale as the phase and shear velocity inversions in order to produce a smooth 2-D crustal thickness map. We divide the crust into three layers with a thin upper crust (one-eighth total crustal thickness), a thicker midcrust (three-eighths total crustal thickness), and a lower crust (one-half total crustal thickness). The uppermost 100 km of the mantle is divided into 10 km thick layers. We divide the next 80 km into layers 20 km thick, and the remainder of the upper mantle to a depth of 400 km is divided into 40 km thick layers. We are most interested in the crustal and uppermost (<300 km) mantle structure, but we allow for changes in velocity to a depth of 400 km to limit potential smearing of the deeper structure into the upper mantle. We use the upper mantle structure of AK135 [*Kennett et al*., 1995] as a starting model, and we fix layer thicknesses in the inversion. Additionally, since the *P* wave velocity has much less influence on the phase velocities than the shear velocity, we fix V_P/V_S ratios at 1.73 for the crust and 1.81 for the upper mantle.

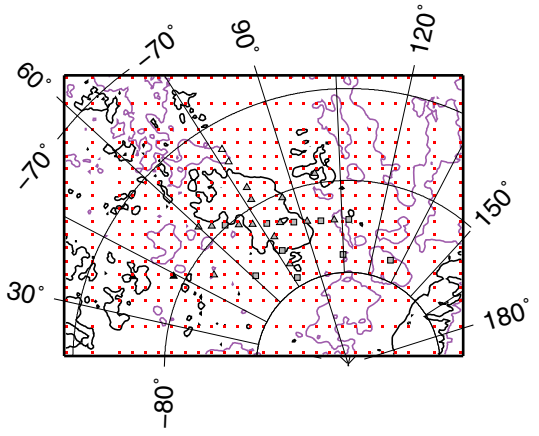

Figure 3. Location of grid nodes (red) used in this study. Black and violet contours are the 1000 and 0 m elevation contours, respectively [*Lythe et al*., 2001]. Stations are plotted as in Figure 1. Inner node spacing is 80 km, and outer node spacing is 160 km.

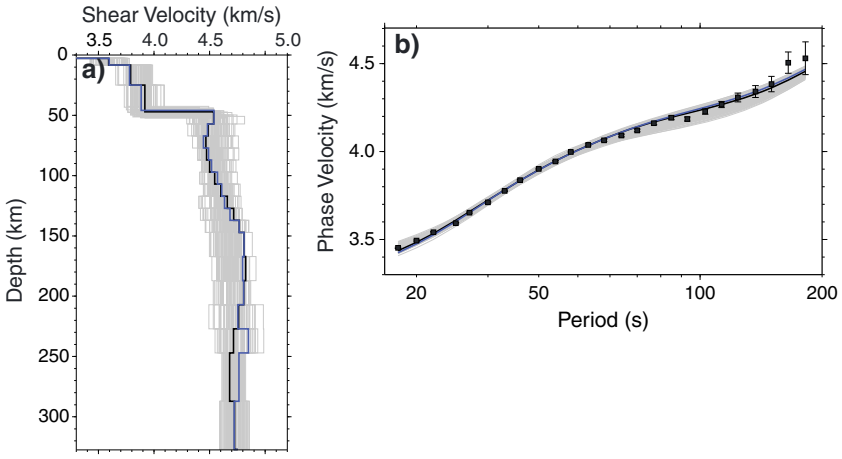

Figure 4. (a) One-dimensional shear velocity structure of the GSM region. Initial inverse model (black) is refined using Monte Carlo modeling to produce acceptable models (grey). Minimum cost model (blue) is used for interpretation. (b) Phase velocities predicted by acceptable shear velocity models from Monte Carlo simulation (grey). Blue line is the phase velocity curve predicted by the minimum cost model. Black squares are results of average phase velocity inversion with 2σ uncertainty bars.

2.3.2. Monte Carlo Modeling

[13] One pitfall of inverting phase velocity data for shear velocity structure is the trade-off between the crustal thickness and the velocity structure of the lowermost crust and the uppermost mantle. In order to better constrain these uncertainties, we conduct a Markov chain Monte Carlo simulation of the model space surrounding the 1-D shear velocity result. Monte Carlo modeling performs a random walk around the initial model to generate a number of acceptable shear velocity models that fit the phase velocity results within an acceptable uncertainty window. The approach has become increasingly common as a means to parameterize uncertainties in shear velocity inversions [*Sambridge and Mosegaard*, 2002]. We parameterize the crust in the same way as in the linear inversion and allow the velocity to vary by 5%. Additionally, we allow for low velocity layers within the crust but fix the velocity in the ice layer. Layer thicknesses are fixed as in the linear inversion, with the exception of the lowermost crust and uppermost mantle layers. Here we allow the layer thicknesses to change by up to 5 km in order to estimate both a best fit crustal thickness and allow for uncertainties in the Moho depth from extrapolation of receiver functions. Shear velocities in the upper 200 km of the mantle is allowed to change by 7% and depths of 200–280 km by 3%. We seek to search the model space around the inverse solution while minimizing the complexity of the model in the mantle. To this end, we attempt to minimize the following equations:

$$C = \chi^2_{\mathrm{red}} \times \sqrt{\mathrm{ISE}} \tag{1}$$

$$\chi^2_{\mathrm{red}} = \frac{1}{N}\sum_{i=1}^{n} \frac{\left(d_i^{\mathrm{obs}} - d_i^{\mathrm{pred}}\right)^2}{\left(\sigma_i^{\mathrm{obs}}\right)^2} \tag{2}$$

$$\mathrm{ISE} = \sum_{j=2}^{m-1} \left(\left[\frac{\Delta v_j^{j+1} - \Delta v_{j-1}^{j}}{\Delta z_j^{j+1} - \Delta z_{j-1}^{j}}\right]_{\mathrm{forward}} - \left[\frac{\Delta v_j^{j+1} - \Delta v_{j-1}^{j}}{\Delta z_j^{j+1} - \Delta z_{j-1}^{j}}\right]_{\mathrm{inverse}} \right)^2 \tag{3}$$

where C is the cost function, χ^2 is the reduced chi-square misfit of the forward phase velocity model to the phase velocity inversion, and ISE is an estimate of model roughness. For χ^2 (2), N is the number of periods, d is the observed or predicted phase velocity at a period i, and σ is the standard deviation of the observed phase velocities. ISE (3) is an estimate of the forward model roughness relative to the inverse model in the mantle. Because an arbitrarily complex model can produce a small χ^2 value, we apply ISE as a weight on χ^2 to ensure that acceptable models are relatively smooth. This parameterization allows for minimizing the misfit of the observed dispersion curve while also limiting complexity in the resulting shear velocity model (Figure 4). To further limit models to those that are geologically reasonable, we limit velocity changes between adjacent layers in the mantle to be twice the maximum velocity step of the mantle in the inverse model. If a velocity model falls within the corridor of acceptable misfits ($7 \times \chi^2_{\mathrm{inverse}}$), we include it in our mean model and uncertainty estimates. In order to limit the effect of varying V_P or density on the models, we fix the V_P/V_S ratio for the crust and the upper mantle to values used in the inverse solution and hold density constant. Because the mean and median velocity models smear structure vertically, limiting the depth resolution of the resulting shear velocity model, we present the best fit model for interpretation purposes.

3. Results

3.1. Phase Velocities

[14] The average phase velocity results obtained in this study (Figure 5) differ greatly from the dispersion curve predicted by the reference model AK135 [*Kennett et al.*, 1995]. We observe phase velocities significantly slower than the global average at 18–40 s. At these periods, our results are slower than other Archean and Proterozoic terranes studied with the two-plane wave method [*Adams and Nyblade*, 2011; *Chen et al.*, 2007]. This is in part due to the thick ice cover in the region which influences short-period phase velocity measurements [*Ritzwoller et al.*, 2001], though

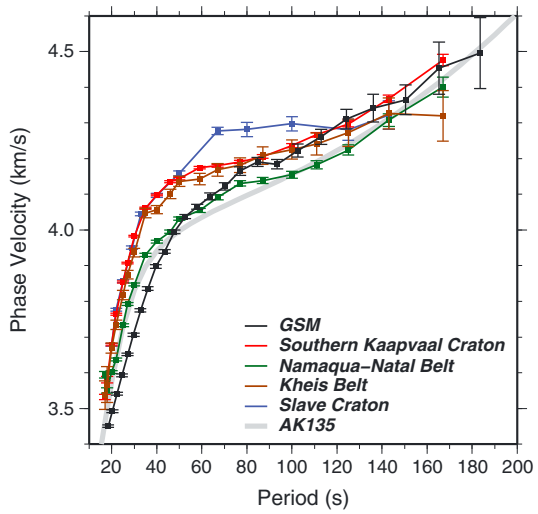

Figure 5. Average phase velocity curve (black) for study region compared to the global average model AK135 (grey) [*Kennett et al*., 1995] and other regions of Archean and Proterozoic ages that have been studied using the two-plane wave method [*Adams and Nyblade*, 2011; *Chen et al*., 2007]. Short-period results are slower than all models, highlighting the thick crust and ice cover of the GSM region. At longer periods (>70 s), the GSM compared favorably with the Archean Kaapvaal craton (red) and the Paleoproterozoic Kheis Belt (brown) [*Adams and Nyblade*, 2011], though it is slower than the Slave craton [*Chen et al*., 2007]. The GSM remains faster than AK135 and the Neoproterozoic/Paleozoic Namaqua-Natal Belt (green) [*Adams and Nyblade*, 2011] across much of the range of periods presented here. Error bars on the y axis are 2σ uncertainties.

thick ice is unable to fully explain the observed velocity anomaly. At longer periods, the GSM phase velocity curve is faster than the global average and similar to regions of Archean and Proterozoic ages. Overall, average phase velocity results indicate a thick crust and a seismically fast upper mantle consistent with a Precambrian origin.

[15] We use the 1-D average dispersion curve as a starting model for 2-D inversions that solve for laterally varying phase velocities. Resulting phase velocity maps and an estimate of a posteriori standard error based on the model covariance matrix are presented in Figure 6. Phase velocities across the region are highly variable at 18 s. We observe slower velocities underlying the Vostok Subglacial Highlands (VSH) and within the GSM and faster velocities beneath the Polar Subglacial Basin (PSB) and LRS (Figure 6a). This pattern is also observed at intermediate periods of 33–44 s. Fast velocities reach a maximum perturbation of 2% at 33 s and correlate well with the inland extension of the LRS (Figure 6b). Slow phase velocities dominate the central region of the GSM, extending from the northeast to the southwest and extend to a period of 77 s (Figure 7f). We attribute most of the phase velocity variations at periods of 33–53 s to variations in crustal thickness, with thinner crust in the LRS and the PSB and thicker crust underlying the GSM. The amplitude of anomalies decreases at longer periods, though we are able to image variations of up to 2% throughout the study region.

[16] Both gravity and receiver function studies of the region indicate a significantly thickened crust exists beneath the core of the GSM [*Block et al*., 2009; *Ferraccioli et al*., 2011; *Hansen et al*., 2010]. In order to ensure that our 2-D phase velocity maps and resulting shear velocity inversions are not impacted by the relatively small region of highly thickened crust, we investigate the effect of using a single, average starting model on our results. We perform inversions using multiple, regional starting models by separating the study region based on shear wave splitting results or crustal thickness. In both cases, 1-D shear velocity results are indistinguishable from the average model within error bounds. Two-dimensional phase velocity maps based on these regionalizations are highly similar to results based on a single starting model.

3.2. Azimuthal Anisotropy

[17] The two-plane wave method allows for the inclusion of an azimuthal anisotropy term. Because we lack information about major tectonic boundaries in the region, we perform inversions for only a single region in our investigation of the GSM (Figure 7). We observe a fast axis that is subparallel to many of the shear wave splitting results for the region [*Hernandez et al*., 2010]. Because we solve for only a single anisotropy value, we are unable to capture the detailed 2-D variations in anisotropy that *Hernandez et al*. [2010] determine using SKS splitting measurements (Figure 7). Overall, we observe approximately 1% anisotropy at periods below 100 s. At longer periods, the uncertainty of the anisotropy measurements increases greatly due to a rapid decrease in raypath coverage. Due to this increased uncertainty, we include but do not interpret azimuthal anisotropy at periods greater than 100 s in phase velocity inversions. We find little difference in phase velocity variations between anisotropic and isotropic inversions at these periods, indicating that velocity results are not biased by the presence of azimuthal anisotropy.

3.3. Shear Velocities

[18] The 1-D average crustal shear velocities range from 3.6 to 3.9 km/s, and the best fit average crustal thickness is 47 km (Figure 4). We find lithospheric mantle that is fast relative to global average models extending to a depth of ~250 km. Three-dimensional shear velocity maps primarily highlight differences in crustal thickness and lithospheric structure. The 30 km depth slice (Figure 8a) has shear velocity values of 3.875–4 km/s across the majority of the study region, with exceptions being the Lambert Rift and Polar Subglacial Basin regions where shear velocities are less than 3.875 km/s. Best fit crustal thicknesses for the Lambert Rift (Figure 9b) are 38–45 km, and crustal thicknesses less than 35 km are observed in the Polar Subglacial Basin. An additional region of crust less than 42.5 km lies between the Vostok Subglacial Highlands and the Subglacial Lake Vostok (Figure 9b). Thinner crust in this region is supported by gravity work in the area of Subglacial Lake Vostok [*Studinger et al*., 2003], though we are unable to match the reported crustal thickness of ~30 km. Shear velocities at depths below the crust are largely homogeneous throughout the study region. We observe shear velocities across the study region ranging from 4.5 to 4.8 km/s at a depth of 150 km, which represents a variation of −2% to

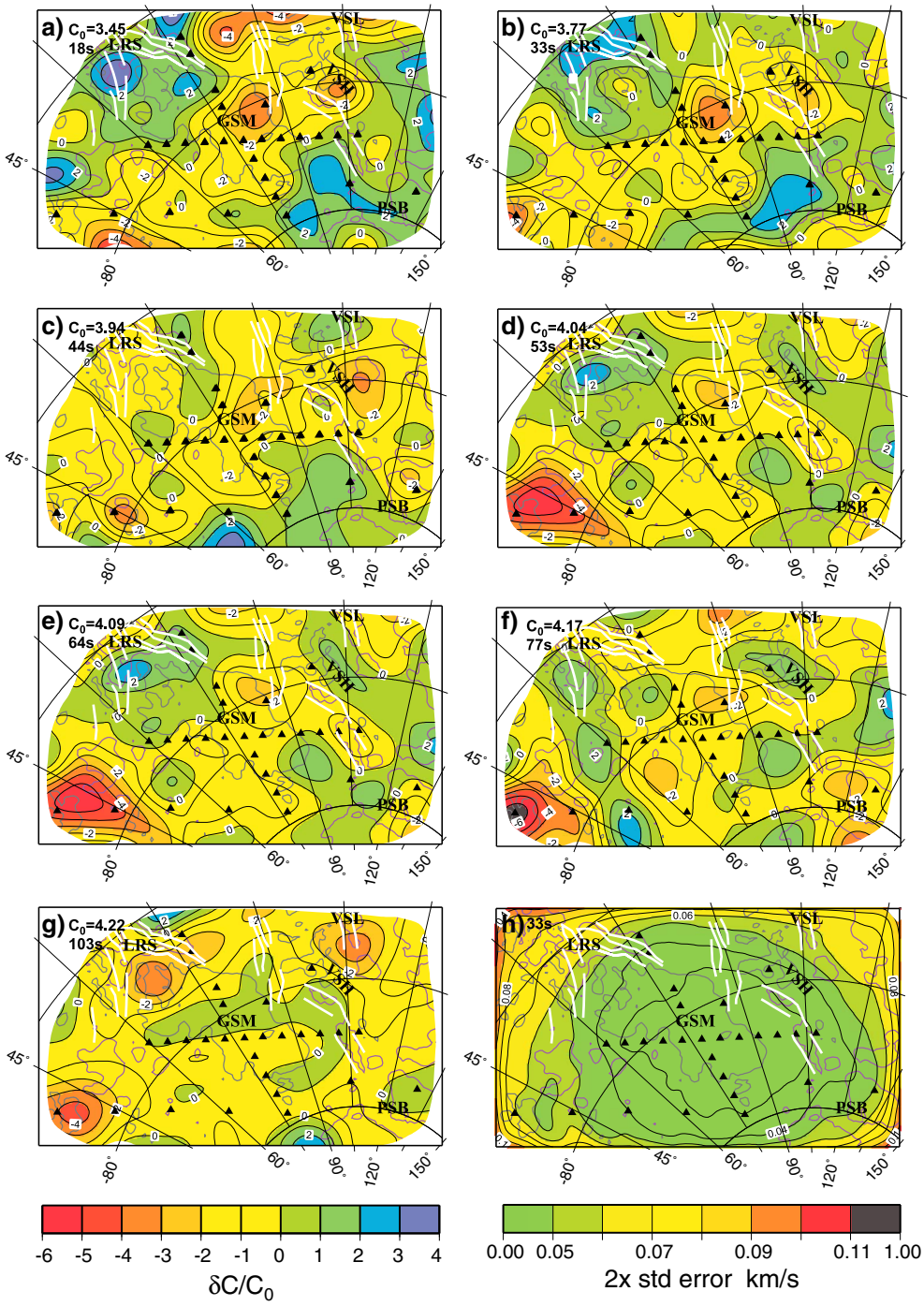

Figure 6. Two-dimensional phase velocity maps for (a) 18, (b) 33, (c) 44, (d) 53, (e) 64, (f) 77, and (g) 103 s periods plotted relative to the 1-D average at each period (upper left corner of map). (h) Standard error map for 33 s. Velocity maps are clipped at the 0.07 km/s standard error contour at 33 s. Station locations are plotted as black triangles, and the 1000 and 0 m bedrock elevation contours are plotted in dark grey and violet, respectively. Mapped rifts from *Ferraccioli et al*. [2011] plotted with heavy white lines. Major subglacial features are labeled as in Figure 1.

+7 % relative to AK135. We note that slow velocities are limited to the LRS and the PSB (Figures 8c and 10b) and that the GSM region is underlain by consistently fast mantle. This indicates that any thermal activity in the mantle has not occurred directly beneath the GSMs and is limited to the periphery of our study area. A region of high shear velocity (>4.75 km/s) is observed extending across the study region at depths of about 250 km (Figure 8d). Shear velocities decrease at depths greater than 250 km, indicating that the seismic lithosphere is limited to shallower depths, a result consistent with globally based studies of the region [*Danesi and Morelli*, 2001; *Ritzwoller et al*., 2001]. We note that

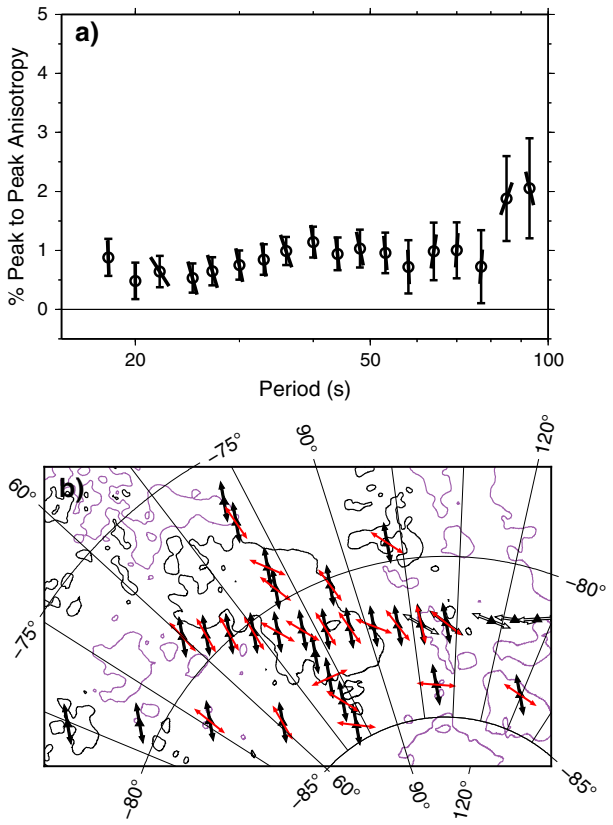

Figure 7. (a) Peak-to-peak azimuthal anisotropy amplitude results for 2-D phase velocity inversions. Anisotropy amplitude is low, i.e., <~1%, for periods shorter than 100 s. Beyond 100 s, amplitudes increase along with uncertainties, likely due to lack of azimuthal coverage, and the isotropic velocity model is preferred. Azimuths are plotted relative to 107.5°E, the false northing direction used in the inversion. (b) Map of fast direction from phase velocities at 53 s compared to published [*Barklage et al*., 2009] (white) and preliminary shear wave splitting results [*Hernandez et al*., 2010] (red). Only fast azimuths are shown for splitting results. We solve only for a single region of anisotropy in our phase velocity inversions. and azimuths are plotted at stations for comparison.

minor variations in seismic velocity correlate with known geologic provinces relatively well (Figures 8 and 10). Uncertainties in shear velocity determined by the Monte Carlo simulation are generally small (see Figure S1 in the supporting information) and highest in the lower crust and uppermost 50 km of mantle.

4. Discussion

[19] Two recent surface wave studies have focused on the Antarctic continent as a whole using data from southern hemisphere stations of the global seismic network. *Ritzwoller et al*. [2001] utilized fundamental-mode phase and group velocities of both Rayleigh and Love waves to perform anisotropic shear velocity tomography of the entire Antarctic continent. They found evidence for thickened crust and a significant lithospheric root beneath the GSM. However, they lacked the resolution (maximum resolution in the GSM was 500–600 km at a period of 50 s and >800 km at a period of 150 s) to image the sharp structural boundaries we observe between the GSM and the Lambert Rift. A more recent study [*Morelli and Danesi*, 2004] has found similar lithospheric thicknesses in the GSM, though it too lacked the resolution to image structural boundaries within East Antarctica. On a broad scale, our results match both studies well, though we observe significantly more variation in crustal thickness than either study. Additionally, we clearly image the inland extension of the Lambert Rift and a significant difference between structures in the GSM and the Polar Subglacial Basin.

4.1. Velocity and Density of the Gamburtsev Crustal Root

[20] We find a significant crustal root centered beneath the highest elevations of the GSM. Our Monte Carlo modeling allows for a ±5 km variation in crustal thickness and reveals results that are close to those determined from receiver functions in the region (Figure 9) [*Hansen et al*., 2009, 2010]. We find that crustal thickness changes in the Monte Carlo simulation result in small (±2 km) changes from the initial model and are well correlated regionally (Figure 9c). The correlation of the regions of thick crust and elevated topography argues in favor of GSM topography being supported by a buoyant crustal root. However, recent gravity modeling of the GSM crustal root [*Ferraccioli et al*., 2011] has suggested that the lowermost crust of the GSM is dominated by high density rocks. *Ferraccioli et al*. [2011] estimated a lower crustal density of 3275 kg/m^3, which is very close to their mantle density of 3300 kg/m^3 and significantly higher than the density of the upper portion of the crust (2800–2900 kg/m^3). This suggests that the crustal root beneath the GSM generates little buoyancy. Such a drastic difference in lower crustal density should be evident in the lower crustal seismic velocities.

[21] In order to assess the effect of high lower crustal densities on seismic velocities, we model seismic velocities based on both lithology and density. *Ferraccioli et al*. [2011] proposed a mafic garnet granulite composition for the lowermost crust. Mafic garnet granulites have a lower average density at lower crustal depths than proposed by the *Ferraccioli et* al. [2011] gravity model, and a density of 3275 kg/m^3 is at the upper end of expected densities for such a lithology [*Christensen and Mooney*, 1995]. Using seismic velocities determined experimentally [*Christensen*, 1996], we find that such a lithology produces a phase velocity curve that fails to fit our results well in comparison to that determined by our shear velocity inversion (Figures 11a and 11b).

[22] If we assume the density structure of *Ferraccioli et al*. [2011] and calculate a seismic velocity directly using the nonlinear velocity/density regression of *Christensen and Mooney* [1995] and reasonable V_P/V_S ratios [*Christensen*, 1996], we would expect to find the following: $V_P = 7.54$ km/s, $V_S = 4.19$ km/s, $\rho = 3275$ kg/m^3, and $V_P/V_S = 1.80$. This shear velocity is 6.3% faster than the shear velocity estimate of 3.94 km/s that we find for the lower crust at depths of 29.5–57.4 km. Additionally, the characteristic jump in velocity, which is used to define the Moho, is not

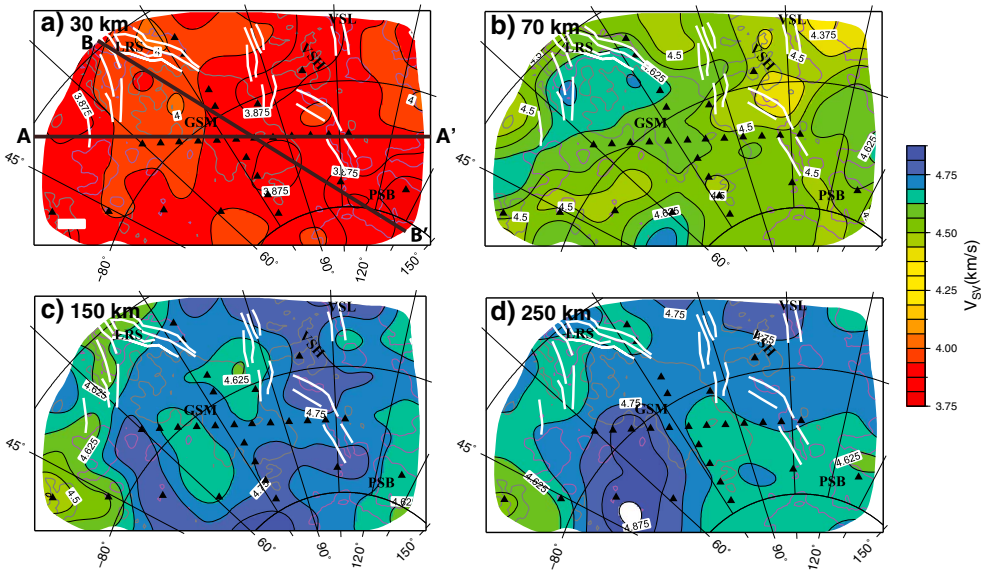

Figure 8. Shear velocity-depth slices at (a) 30 km, (b) 70 km, (c) 150 km, and (d) 250 km. Shear velocity structure in the crust is largely homogeneous in Figure 8a. Uppermost mantle velocities in Figure 8b vary across the study region. The fastest velocities are observed beneath the northern GSM near the LRS. Slow velocities are observed beneath the VSH and the PSB. Velocities in the LRS and the PSB are slower than beneath the GSM at 150 km in Figure 8c. Seismic velocities are largely homogeneous by 250 km in Figure 8d. Rifts mapped by *Ferraccioli et al*. [2011] plotted with heavy white lines. Locations of cross sections (Figure 10) are marked in Figure 8a.

located at the base of this layer (Figure 11c). Rather, there are two large velocity jumps, one corresponding to the middle/lower crustal boundary and another corresponding to the Moho. It is probable that two such large discontinuities would have been apparent in the receiver function analysis of *Hansen et al*. [2010].

4.2. Lithospheric Age Constraints

[23] The ages of the rocks comprising the GSM and East Antarctica are essential for reconstructing the history of the Antarctic continent. While we are unable to investigate the lithology of the region directly, we do find evidence for a Precambrian origin of the GSM lithosphere. Globally, regions of similar tectonic age have been shown to exhibit remarkable similarities in the lithospheric velocity structure [*Lekic and Romanowicz*, 2011; *Poupinet and Shapiro*, 2009]. We compare our average phase velocity curve for the GSM region to those of differing ages using a global phase velocity structure [*Visser et al*., 2008] and a simplified crustal age map [*Mooney et al*., 1998]. We group all phase velocity curves for a given crustal age and calculate the median phase velocity curve. The median phase velocity curve is used in an attempt to account for the different tectonic histories of regions with similar ages globally. The least squares misfit between the median curve for each age and our average phase velocity curve is then calculated with an aim at constraining the age of the GSM lithospheric mantle. We exclude oceanic basins and regions south of 60°S from our analysis. While this analysis does not place an absolute age constraint on the formation of the GSM lithospheric root, it does provide bounds on its formation and informs any attempt at interpreting the evolution of the GSM region.

[24] We compare our results at periods from 50 to 175 s to emphasize similarities in the upper mantle structure and exclude shorter-period phase velocities that are highly sensitive to crustal thickness and structure that vary between different regions. Our phase velocities at these periods correlate best with regions having a tectonothermal age of Paleoproterozoic-Mesoproterozoic (2500–1700 Ma), with slightly poorer fits for regions of Archean (>2500 Ma) and a classification known as "undifferentiated" Precambrian (Figure 12), a classification that encompasses regions of Proterozoic aged crust that have significant Phanerozoic sedimentary cover [*Artemieva et al*., 2004; *Mooney et al*., 1998; *Poupinet and Shapiro*, 2009]. The age determined from this analysis is consistent with recent tectonic reconstructions of the region [*Boger*, 2011; *Veevers and Saeed*, 2008]. Our analysis encompasses a large region of East Antarctica, and it is possible that there are multiple, small cratonic blocks with the study region. Additionally, regions such as the Lambert Rift have undergone Phanerozoic extension, which likely modified the upper mantle, limiting our ability to resolve the lithospheric age to a specific period within the Precambrian. The region as a whole, however, is consistent with an Archean–Mesoproterozoic origin.

[25] The analysis described above also allows us to compare our results with those of differing ages spatially (Figure 13). For each two degrees square used in determining the tectonothermal age [*Bassin et al*., 2000; *Mooney et al*., 1998], we extract a phase velocity curve from the global phase velocity model [*Visser et al*., 2008]. If the misfit between this phase velocity curve and our average model is less than the misfit between the best median model, that of the Paleoproterozoic-Mesoproterozoic age, we

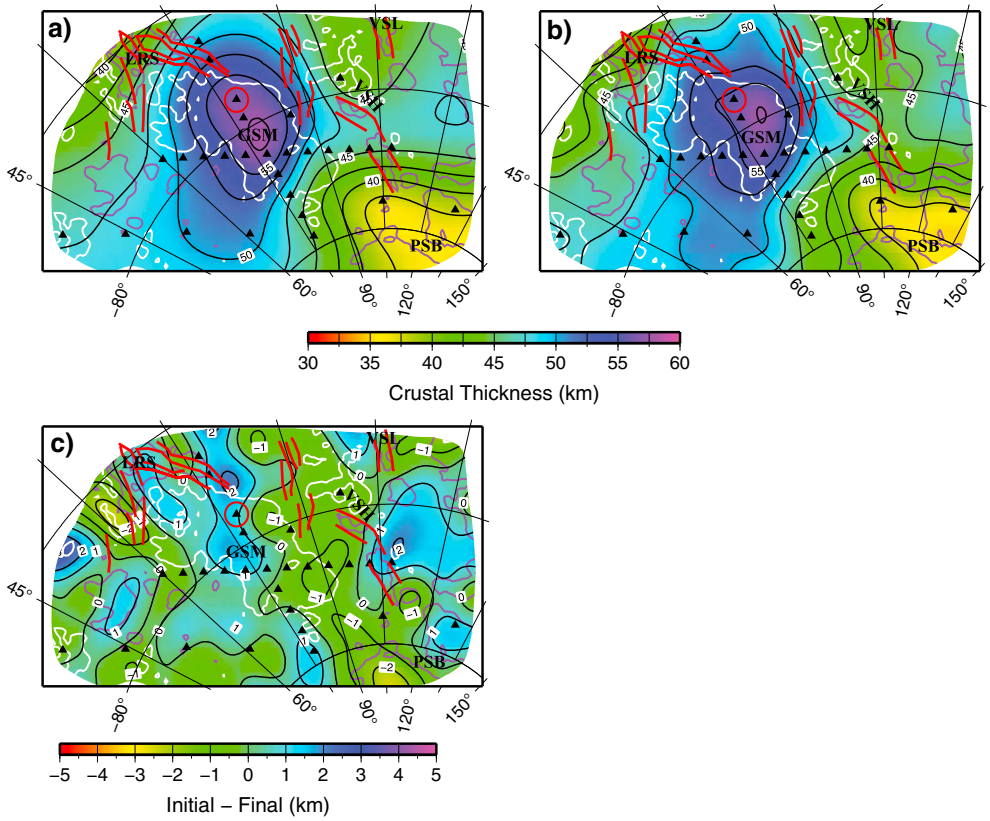

Figure 9. Crustal thickness map from (a) interpolation of receiver functions and (b) Monte Carlo simulation for crustal thickness and shear velocity. The GSM are underlain by a large region with crustal thickness in excess of 48 km, reaching a high of 57 km. Crustal thicknesses of the PSB and the LRS are significantly lower than those of the adjacent regions. (c) Changes in crustal thickness are small and well correlated spatially. Station P124 (circled) is used in comparing the shear velocity structure with the gravity model of *Ferraccioli et al*. [2011]. Rifts mapped by *Ferraccioli et al*. [2011] plotted with heavy red lines.

include it in our map. In this way, we produce a map of locations on Earth that represent an improvement on the best fitting median age curve. Results from this analysis indicate that the GSM phase velocity structure compares favorably with parts of southern and western Africa and Australia. Notably absent from the regions of acceptable misfit are locations of recent mountain building and crustal thickening such as the Andes or Himalayas. The only regions of Phanerozoic age are easternmost North America, where the age map may not accurately reflect the lithospheric structure, and the Southern Urals, where the adjacent Proterozoic lithosphere may influence results. It is unlikely, therefore, that the GSM lithosphere has undergone significant reworking in the last 543 Ma.

[26] A number of recent studies have used the two-plane wave method [*Adams and Nyblade*, 2011; *Adams et al*., 2012; *Chen et al*., 2007] or two-dimensional ray tracing [*Bruneton et al*., 2004] to determine the shear velocity structure of Precambrian terranes. A comparison of the 1-D shear velocity models of the GSM with these regions is therefore instructive. Our results compare favorably with these studies (Figure 14). All models have a seismically fast upper mantle, though they differ in lithospheric thickness. The details of the individual models vary significantly, and our results plot near the center of the surveyed study regions. It is likely that there are several reasons for differences between our models and the models of other researchers. Because we lack geologic constraints on the history and structure of the study area, our results assume a single tectonic history and age for the entire study area, which is unlikely. Additionally, differences in inversion methods and parameterizations in other studies limit direct comparison. We note that there is particularly good fit between our results and the upper 50 km of mantle in the Proterozoic Namaqua-Natal Belt [*Adams and Nyblade*, 2011]. The model of *Chen et al*. [2007] for the Slave Craton and *Bruneton et al*. [2004] for the Baltic Shield are similar at greater depth, though they find a faster uppermost mantle and a thinner seismic lithosphere. Cratons that are currently or have previously undergone thermal modification of their lithospheric roots are significantly different than that of the GSM [*Adams et al*., 2012].

4.3. Preservation of Topography and Formation of the Modern GSM

[27] Our results indicate that a thickened crust underlies the GSM, and the seismically fast upper mantle within the region is consistent with an Archean–Mesoproterozoic origin for the lithosphere. Mesozoic or Cenozoic tectonism should be apparent in our results as a region of slow velocity

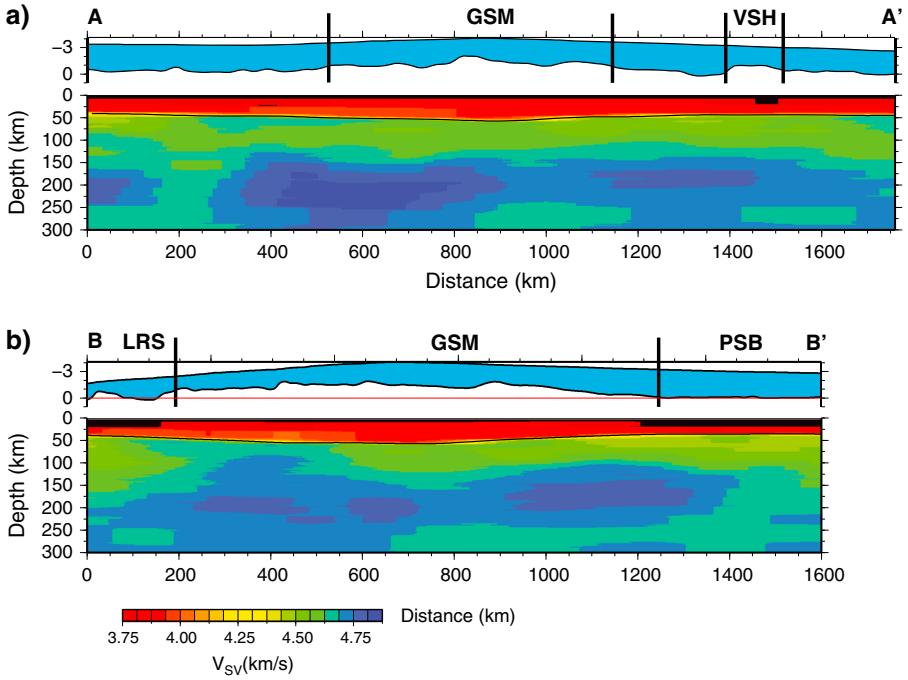

Figure 10. Cross sections of the GSM shear velocity structure. Upper cross sections in both (a) and (b) show surface topography and underlying bedrock topography (note the change in scale). (a) A-A′ is roughly parallel to the N line (N-S) of seismic stations and crosses the break in the lithospheric structure (100–300 km) related to the extension of the Lambert Rift System. (b) Cross section taken diagonally from the Lambert Rift System (LRS) to the Polar Subglacial Basin (PSB). The lithosphere is relatively unbroken across the GSM. The highest seismic velocities are observed beneath the GSM at depths of ~150–250 km.

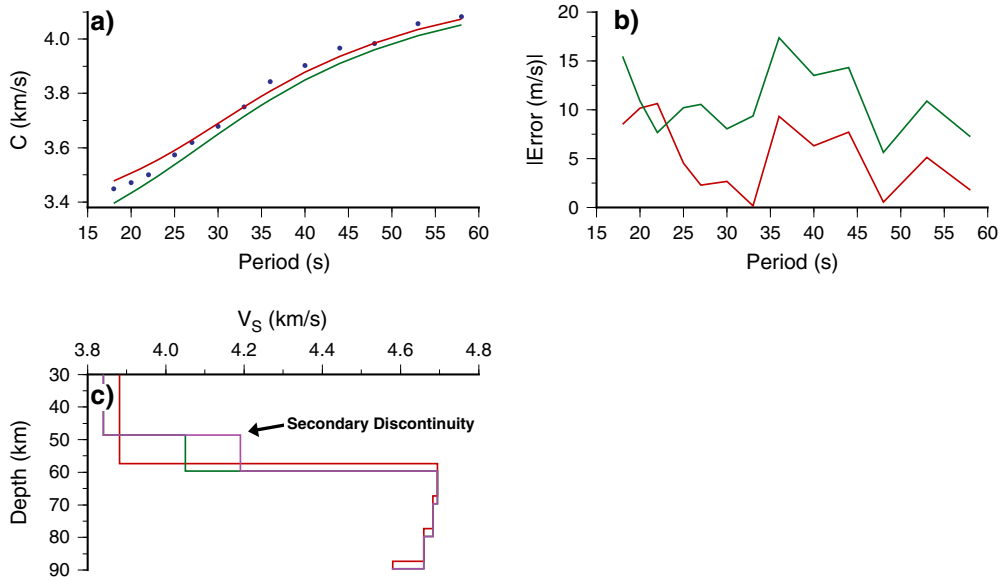

Figure 11. (a) Phase velocity curves predicted by the gravity model with a mafic garnet granulite lithology (green) and shear velocity inversion (red) from this study at seismic station P124 (circled in Figure 9) compared with phase velocity curve measured at station (blue squares). (b) Error of inverse (red) and mafic garnet granulite (green) models relative to phase velocity data reveals significantly higher misfit for the model of *Ferraccioli et al*. [2011], particularly for periods of 25–58 s, a period range that is sensitive to the crustal structure. (c) A comparison of shear velocity models reveals that converting the density structure of *Ferraccioli et al*. [2011] to shear velocity (violet) directly introduces a large secondary velocity jump not observed in the mafic garnet granulite model (green) or the inverse model (red). Upper crustal velocity models for density structure (violet) and mafic garnet granulite (green) overlap in the upper crust.

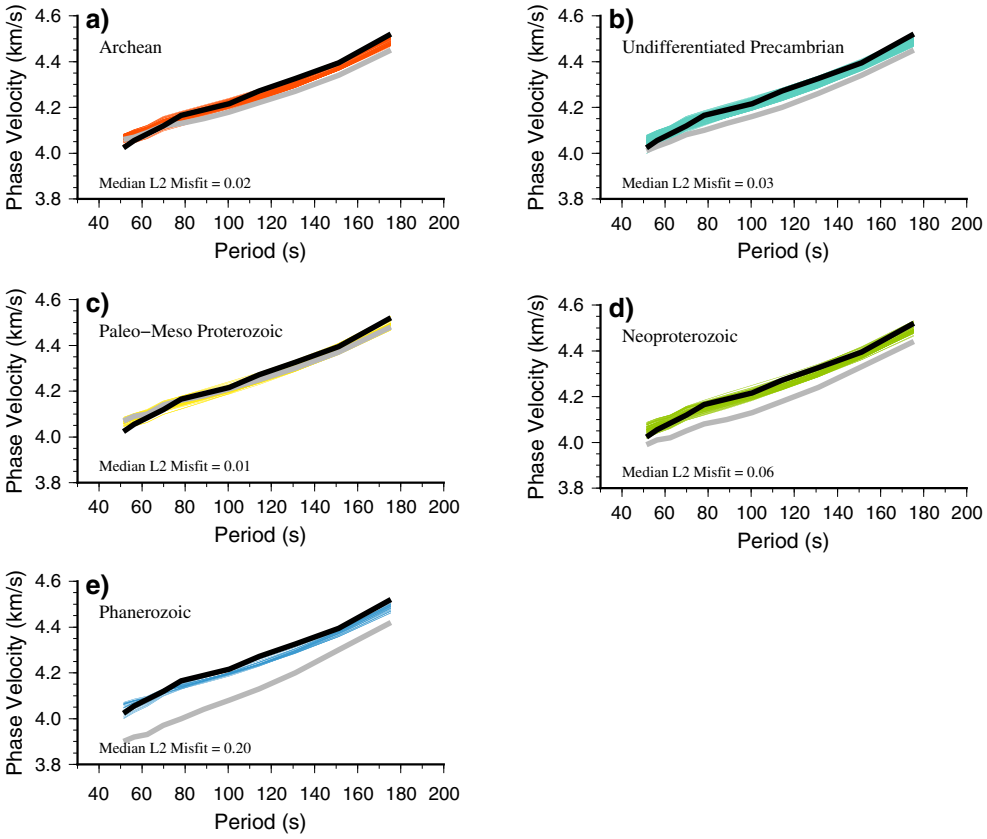

Figure 12. (a–e) Comparison of average phase velocity result from this study (black line) with global median for regions of differing ages (grey lines) using the phase velocity model of *Visser et al*. [2008] reveals a best fit lithospheric age in the Paleoproterozoic-Mesoproterozoic in Figure 12c with a close fit to the Archean in Figure 12a as well. Tectonothermal ages are simplified after *Mooney et al*. [1998]. Least squares misfit between global median and average phase velocity here is listed in each subplot for each tectonothermal age. Colored lines in each subplot are phase velocity curves for locations plotted in Figure 13.

relative to the regional average. The GSM region as a whole is seismically fast to depths of ~250 km with the exception of the LRS and the PSB, which are somewhat slower. In all, we do not observe evidence for thermal or chemical rejuvenation of the lithosphere in the GSM region, particularly underlying or directly abutting the mountain range (Figures 8 and 10). It is true that long-period Rayleigh waves provide limited spatial resolution, and a small slower region may remain unresolved in this study, but a companion body wave tomography study provides higher lateral

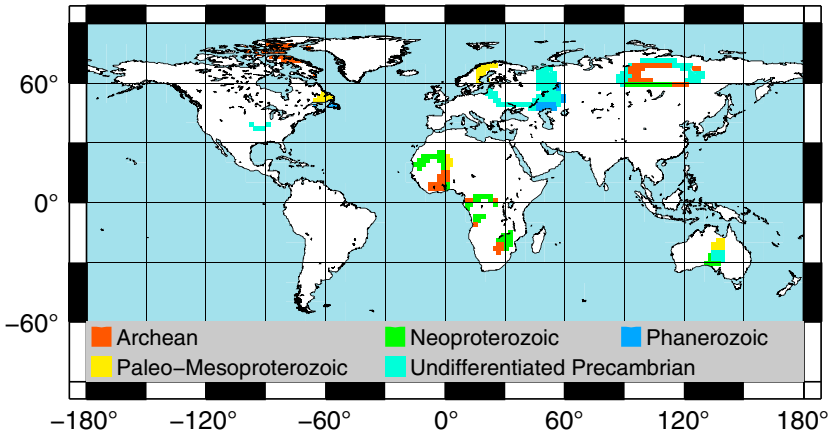

Figure 13. Map of locations plotted as colored lines in phase velocity curves has least squares misfit less than that of the global median for a Paleoproterozoic-Mesoproterozoic age. Southern and western Africa and Australia are close matches to the lithosphere of the GSM. Region south of −60° latitude is not analyzed due to high uncertainties in tectonothermal ages.

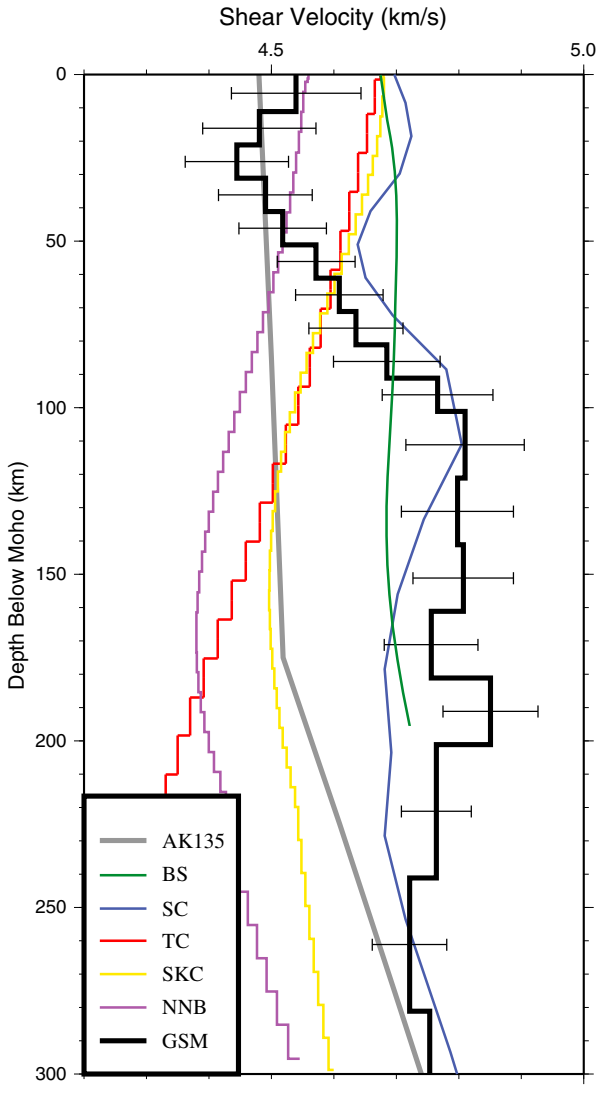

Figure 14. Comparison of 1-D shear velocity structure of the GSM mantle with selected Archean and Proterozoic regions globally; the Slave craton (SC) (blue) [*Chen et al*., 2007], the Baltic shield (BS) (green) [*Bruneton et al*., 2004], the Tanzania craton (TC) (red) [*Adams et al*., 2012], the Kaapvaal craton (SKC) (yellow), and the Proterozoic western Namaqua-Natal belt (NNB) (violet) [*Adams and Nyblade*, 2011]. The GSM (black) region compares favorably with the Slave craton and the Baltic shield but differs greatly from the Tanzania craton, which is surrounded by the East African Rift System. The AK135 global reference model [*Kennett et al*., 1995] is plotted in grey for comparison.

resolution along the two seismic lines and also finds relatively uniform fast velocities [*Lloyd et al*., 2013]. Any model for the formation of the modern GSM must take into consideration the seismically fast upper mantle.

[28] We propose a hybrid model for formation of the GSM in which extremely low long-term erosion rates are coupled with repeated instances of uplift during the Proterozoic–early Paleozoic followed by reactivation of crustal faults during the formation of Pangaea during the late Paleozoic or the Mesozoic breakup of Gondwana. This model is capable of producing both observed crustal thicknesses and topographic relief.

[29] Climate models indicate that the GSM have been ice covered for at least the past 34 Ma [*DeConto and Pollard*, 2003a, 2003b]. In order to preserve topography in excess of 2 km and crustal thickness in excess of 55 km in the central GSM, multiple factors are likely involved. Surface processes must act to limit erosion of the GSM, and processes within the lowermost crust and the upper mantle must limit degradation of the crustal root in order to maintain crustal buoyancy. Crustal thickness estimates from receiver function analysis and this study indicate that erosion within the GSM must be extremely low if the mountains are of any significant age. Recent ground-based radar work has found large, deeply incised valleys in the central GSM consistent with glacial steepening of existing stream valleys [*Bo et al*., 2009]. Long-term erosion rates have been estimated to be as low as 0.01–0.02 km/Ma for the last 250 Ma [*Cox et al*., 2010]. This would correspond to the removal of 2.5–5 km of crustal material from the GSM over this period. Using some simple assumptions about the age and crustal thickness of the GSM, we can extrapolate these results further into the past. The GSM region has a maximum crustal thickness of ~57 km [*Hansen et al*., 2010]. If we assume an original crustal thickness of 70 km, an average crustal density of 2800 kg/m^3, and an end to mountain building processes at 480 Ma based on detrital zircons [*van de Flierdt et al*., 2008], then we can infer a maximum average erosion rate of 0.027 km/Ma. This value is significantly higher than the estimate for the last 250 Ma and more than 10 times that determined to be appropriate for the last 118 Ma for sediment thicknesses in Prydz Bay [*Jamieson et al*., 2005].

[30] Preservation of significant topographic relief over a period of several hundred million years requires processes other than a low erosion rate to be active. The buoyancy force of crustal roots declines over geologic time [*Fischer*, 2002], and they can be removed entirely through the processes of post-orogenic collapse and lithospheric delamination [*Fischer*, 2002; *Kay and Kay*, 1993; *Leech*, 2001]. In order to maintain a buoyant crustal root over the time scale suggested by *van de Flierdt et al*. [2008], the process of post orogenic collapse must be limited. *Leech* [2001] proposed that this process could occur under "dry" conditions when insufficient fluid is present to complete the eclogitization of the lower crust. Additionally, numerical modeling of crustal roots has shown that high viscosity in the lithosphere can aid in the preservation of crustal roots over long periods [*Koyi et al*., 1999; *Marotta et al*., 1998; *Schott and Schmeling*, 1998]. Preservation of thickened crust has been observed in Paleoproterozoic collisional zones throughout the world [*Bruneton et al*., 2004; *Chulick and Mooney*, 2002; *White et al*., 2005; *Zelt and Ellis*, 1999]. These regions, however, exhibit little of the topographic relief observed in the GSM, due to a decline in lower crustal buoyancy over time [*Fischer*, 2002; *French et al*., 2009].

[31] Topographic relief within the GSM is unlikely to be solely related to crustal thickening and uplift during the Neoproterozoic–early Paleozoic. A more likely hypothesis is a hybrid model in which initial crustal thickening occurred intermittently during the assembly of cratonic blocks

throughout the Proterozoic culminating in the formation of Gondwana. Subsequent uplift coincided with the formation of Pangaea during the Carboniferous and Permian and consisted of compression on existing faults and/or compression on a diffuse plate boundary during the Mesozoic breakup of Gondwana. Significant extension of the region is unlikely to have occurred, as the continental lithosphere that underlies the region shows no evidence of thinning.

[32] Compressional uplift may have occurred within the GSM region during the Mesozoic breakup of Gondwana. This is possible if the GSM region served as a diffuse plate boundary for two halves of East Antarctica. In this model, a pole of rotation for the two halves of East Antarctica is located within the continent itself. The presence of the pole of rotation within the plate imposes a torque within the diffuse boundary zone, allowing for compression in the GSM and extension in the LRS [*Zatman et al*., 2001; *Zatman and Richards*, 2002]. Uplift would have terminated when the plate boundary in the Southern Ocean moved far enough away from the continental interior to reduce compressional stresses within the GSM. Such a model reduces the need for extremely low erosion rates existing for >250 Ma or significant transtensional uplift associated with Cretaceous rifting [*Ferraccioli et al*., 2011; *Phillips and Läufer*, 2009]. Such diffuse compression is hypothesized for parts of southern and eastern Africa as the Somali plate separates from the Nubian plate [*Stamps et al*., 2008] and the Indo-Australian plate near Sumatra [*Yue et al*., 2012].

5. Conclusions

[33] Questions regarding the age, provenance, and history of the Gamburtsev Subglacial Mountains have plagued Antarctic researchers since their discovery during the 1950s. We have conducted shear velocity tomography based on teleseismic Rayleigh waves to image the crust and upper mantle structure of the GSM at an unprecedented scale. We are able to identify three seismically distinct regions in the study region. The LRS extends from the extreme northwest of the study region south toward the South Pole on the western edge of the GSM. A thickened crust and a lithospheric root that extends to a depth of about 250 km underlie the Gamburtsev Subglacial Mountains. A thin crust and mantle velocities that are slower than the GSM characterize the PSB region in the southeast of the study region. Furthermore, we have determined an approximate age for the formation of the observed lithospheric root beneath the GSM. We suggest that the Gamburtsev Subglacial Mountains have served as a region repeated continental shortening since their initial formation. The lithosphere of the GSM region stabilized following the formation of the East Antarctic craton during the Archean and Paleoproterozoic. Intracratonic shortening occurred during the Neoproterozoic and early Paleozoic coinciding with the assembly of Gondwana and finally during the development of Pangaea during the late Paleozoic and/or on a diffuse plate boundary during the Mesozoic breakup of Gondwana. Long-term, cold-based glaciation following the most recent uplift event, combined with a thick, high viscosity lithospheric root, has limited erosion of the GSM from the top and delamination/ductile rebound from the base. Consistent with the recent receiver function analysis, we find no evidence for an anomalously dense crustal root, and shear velocity results for the upper mantle do not indicate significant lithospheric thinning as might be expected in a heavily rifted environment.

[34] **Acknowledgments.** The authors wish to acknowledge the hard work and support of the field teams responsible for collecting these data. We wish to thank the staff and polar support specialists at IRIS/PASSCAL, who provided both instrumentation and field support during the operation of this array, and the pilots and staff of Kenn Borek Air and the New York Air National Guard for flight support. We thank Raytheon Polar Services and staff at South Pole Station, McMurdo Station, and AGAP-S camp for logistical support. This project was funded by U.S. NSF grants ANT-0537597, ANT-0537371, ANT-0838934, and ANT-0838973, the NIPR of Japan, and the China National Science Foundation grant NSFC-40874201. Figures in this paper were produced using GMT [*Wessel and Smith*, 1998]. We thank two anonymous reviewers for the helpful and constructive comments.

References

Adams, A., and A. Nyblade (2011), Shear wave velocity structure of the southern African upper mantle with implications for the uplift of southern Africa, *Geophys. J. Int.*, 1–17. doi:10.1111/j.1365-246X.2011.05072.x.

Adams, A., A. Nyblade, and D. S. Weeraratne (2012), Upper mantle shear wave velocity structure beneath the East African plateau: Evidence for a deep, plateau-wide low velocity anomaly, *Geophys. J. Int.*, *189*, 123–142. doi:10.1111/j.1365-246X.2012.05373.x.

Artemieva, I. M., M. Billien, J.-J. Levaeque, and W. D. Mooney (2004), Shear wave velocity, seismic attenuation, and thermal structure of the continental upper mantle, *Geophys. J. Int.*, *157*, 607–628. doi:10.1111/j.1365-246X.2004.02195.x.

Barklage, M., D. A. Wiens, A. Nyblade, and S. Anandakrishnan (2009), Upper mantle seismic anisotropy of South Victoria Land and the Ross Sea coast, Antarctica from SKS and SKKS splitting analysis, *Geophys. J. Int.*, *178*, 729–741. doi:10.1111/j.1365-246X.2009.04158.x.

Bassin, C., G. Laske, and G. Masters (2000), The current limits of resolution for surface wave tomography in North America, *Eos Trans. AGU*, *81*(48), Fall Meet. Suppl., Abstract S12A-03.

Bell, R. E. et al. (2011), Widespread persistent thickening of the East Antarctic Ice Sheet by freezing from the base, *Science*, *331*, 1592–1595. doi:10.1126/science.1200109.

Block, A. E., R. E. Bell, and M. Studinger (2009), Antarctic crustal thickness from satellite gravity: Implications for the Transantarctic and Gamburtsev Subglacial Mountains, *Earth Planet. Sci. Lett.*, *288*, 194–203. doi:10.1016/j.epsl.2009.09.022.

Bo, S., M. J. Seigert, S. M. Mudd, D. Sugden, S. Fujita, C. Xianbin, J. Yunyun, T. Xueyuan, and L. Yuansheng (2009), The Gamburtsev mountains and the origin and early evolution of the Antarctic Ice Sheet, *Nature*, *459*, 690–693. doi:10.1038/nature08024.

Boger, S. D. (2011), Antarctica—Before and after Gondwana, *Precambrian Res.*, *19*, 335–371. doi:10.1016/j.gr.2010.09.003.

Bruneton, M., et al. (2004), Complex lithospheric structure under the central Baltic Shield from surface wave tomography, *J. Geophys. Res.*, *109*, B10303, doi:10.1029/2003JB002947.

Chen, C.-W., S. Rondenay, D. S. Weeraratne, and D. B. Snyder (2007), New constraints on the upper mantle structure of the Slave craton from Rayleigh wave inversion, *Geophys. Res. Lett.*, *34*, L10301, doi:10.1029/2007GL029535.

Christensen, N. I. (1996), Poisson's ratio and crustal seismology, *J. Geophys. Res.*, *101*(B2), 3139–3156.

Christensen, N. I., and W. D. Mooney (1995), Seismic velocity structure and composition of the continental crust: A global review, *J. Geophys. Res.*, *100*(B7), 9761–9788.

Chulick, G. S., and W. D. Mooney (2002), Seismic structure of the crust and uppermost mantle of North America and adjacent oceanic basins: A synthesis, *Bull. Seismol. Soc. Am.*, *92*(6), 2478–2492, doi:10.1785/. 0120010188.

Cox, S. E., S. N. Thomson, P. W. Reiners, S. R. Hemming, and T. van de Flierdt (2010), Extremely low long-term erosion rates around the Gamburtsev Mountains in interior East Antarctica, *Geophys. Res. Lett.*, *37*, L22307, doi:10.1029/2010GL045106.

Danesi, S., and A. Morelli (2001), Structure of the upper mantle under the Antarctic Plate from surface wave tomography, *Geophys. Res. Lett.*, *28*(23), 4395–4398.

DeConto, R. M., and D. Pollard (2003a), A coupled climate-ice sheet modeling approach to Early Cenozoic history of the Antarctic ice sheet, *Palaeogeogr. Palaeoclimatol. Palaeoecol.*, *198*, 39–52. doi:10.1016/S0031-0182(03)00393-6.

DeConto, R. M., and D. Pollard (2003b), Rapid Cenozoic glaciation of Antarctica induced by declining atmospheric CO_2, *Nature*, *421*, 245–249. doi:10.1038/nature01290.

Ferraccioli, F., C. A. Finn, T. A. Jordan, R. E. Bell, L. M. Anderson, and D. Damaske (2011), East Antarctic rifting triggers uplift of the Gamburtsev Mountains, *Nature*, *479*, 388–392. doi:10.1038/nature10566.

Fischer, K. M. (2002), Waning buoyancy in the crustal roots of old mountains, *Nature*, *417*, 933–936, doi:10.1038/nature00855.

Fitzsimons, I. C. W. (2000), Grenville-age basement provinces in East Antarctica: Evidence for three separate collisional orogens, *Geology*, *28* (10), 879–882. doi:10.1130/0091-7613(2000)28<879:GBPIEA>2.0.CO;2.

Fitzsimons, I. C. W. (2003), Proterozoic basement provinces in southern and southwestern Australia, and their correlation with Antarctica, in *Proterozoic East Gondwana: Supercontinent Assembly and Breakup*, edited by M. Yoshida, B. F. Windley, and S. Dasgupta, pp. 93–130, Geol. Soc. London Spec. Publ., London.

Forsyth, D. W., and A. Li (2005), Array analysis of two-dimensional variations in surface wave phase velocity and azimuthal anisotropy in the presence of multipathing interference, in *Seismic Earth: Array Analysis of Broadband Seismograms*, edited by A. Levander and G. Nolet, pp. 81–97, AGU, Washington, D. C.

French, S. W., K. M. Fischer, E. M. Syracuse, and M. E. Wysession (2009), Crustal structure beneath the Florida-to-Edmonton broadband seismometer array, *Geophys. Res. Lett.*, *36*, L08309, doi:10.1029/2008GL036331.

Fretwell, P., et al. (2013), Bedmap2: Improved ice bed, surface and thickness datasets for Antarctica, Cryosphere, *7*, 375–393, doi:10.5194/tc-7-375-2013.

Hansen, S. E., J. Julia`, A. A. Nyblade, M. L. Pyle, D. A. Wiens, and S. Anandakrishnan (2009), Using *S* wave receiver functions to estimate crustal structure beneath ice sheets: An application to the Transantarctic Mountains and East Antarctic craton, *Geochem. Geophys. Geosyst.*, *10* (8), Q08014, doi:10.1029/2009GC002576.

Hansen, S. E., A. A. Nyblade, D. S. Heeszel, D. A. Wiens, P. J. Shore, and M. Kanao (2010), Crustal structure of the Gamburtsev Mountains, East Antarctica, from S-wave receiver functions and Rayleigh wave phase velocities, *Earth Planet. Sci. Lett.*, *300*, 395–401. doi:10.1016/j.epsl.2010.10.022.

Hernandez, S., D. A. Wiens, and A. Nyblade (2010), East Antarctic seismic anisotropy from Shear-wave splitting analysis of AGAP seismograms, *Abstract DI13A-1849 presented at the 2010 Fall Meeting, AGU, San Francisco, Calif., 13–17 Dec*.

Herrmann, R. B., and C. J. Ammon (2002), Computer Programs in Seismology: Surface Waves, Receiver Functions and Crustal Structure, p. 110, St. Louis Univ., St. Louis, Mo.

Jamieson, S. S. R., N. R. J. Hulton, D. Sugden, A. J. Payne, and J. Taylor (2005), Cenozoic landscape evolution of the Lambert Basin, East Antarctica: The relative role of rivers and ice sheets, *Global Planet. Change*, *45*, 35–49, doi:10.1016/j.gloplacha.2004.09.015.

Johns, B., K. R. Anderson, B. C. Beaudoin, J. Fowler, T. Parker, and S. White (2006), Development of a power and communications system for remote autonomous polar observations, *Eos Trans. AGU*, *87*(52), Fall Meet. Suppl., Abstract S41A-1314.

Kay, R. W., and S. M. Kay (1993), Delamination and delamination magmatism, *Tectonophysics*, *219*, 177–189.

Kennett, B. L. N., E. R. Enghdal, and R. Buland (1995), Constraints on seismic velocities in the Earth from travel times, *Geophys. J. Int.*, *122*, 108–124.

Koyi, H. A., A. G. Milnes, H. Schmeling, C. J. Talbot, C. Juhlin, and H. Zeyen (1999), Numerical models of ductile rebound of crustal roots beneath mountain belts, *Geophys. J. Int.*, *139*, 556–562.

Leech, M. L. (2001), Arrested orogenic development: eclogitization, delamination, and tectonic collapse, *Earth Planet. Sci. Lett.*, *185*, 149–159.

Lekic, V., and B. Romanowicz (2011), Tectonic regionalization without a priori information: A cluster analysis of upper mantle tomography, *Earth Planet. Sci. Lett.*, *301*, 151–160. doi:10.1016/j.epsl.2011.05.050.

Li, A., D. W. Forsyth, and K. M. Fischer (2003), Shear velocity structure and azimuthal anisotropy beneath eastern North America from Rayleigh wave inversion, *J. Geophys. Res.*, *108*(B8), 2362, doi:10.1029/2002JB002259.

Lisker, F., R. Brown, and D. Fabel (2003), Denudational and thermal history along a transect across the Lambert Graben, northern Prince Charles Mountains, Antarctica, derived from apatite fission track thermochronology, *Tectonics*, *22*(5), 1055, doi:10.1029/2002TC001477.

Liu, X., Y. Zhao, and X. Liu (2002), Geological aspects of the Grove Mountains, East Antarctica, *Bull. R. Soc. N. Z.*, *35*, 161–166.

Liu, X., J. Hu, Y. Zhao, Y. Lou, C. Wei, and X. Liu (2009), Late Neoproterozoic/Cambrian high-pressure mafic granulites from the Grove Mountains, East Antarctica: *P-T-t* path, collisional orogeny and implications for assembly of East Gondwana, *Precambrian Res.*, *174*, 181–199. doi:10.1016/j.precamres.2009.07.001.

Lloyd, A. J., A. A. Nyblade, D. A. Wiens, S. E. Hansen, M. Kanao, P. J. Shore, and D. Zhao (2013), Upper mantle seismic structure beneath central East Antarctica from body wave tomography: Implications for the origin of the Gamburtsev Subglacial Mountains, *Geochem. Geophys. Geosys.*, doi:10.1002/ggge.20098, in press.

Lythe, M. B., D. G. Vaughan, and t. B. Consortium (2001), BEDMAP: A new ice thickness and subglacial topographic model of Antarctica, *J. Geophys. Res.*, *106*(B6), 11335–11351.

Marotta, A. M., M. Fernandez, and R. Sabadini (1998), mantle unrooting in collisional settings, *Tectonophysics*, *296*, 31–46.

Mooney, W. D., G. Laske, and T. G. Masters (1998), Crust 5.1: A global crustal model at 5 × 5, *J. Geophys. Res.*, *103*(B1), 727–747.

Morelli, A., and S. Danesi (2004), Seismological imaging of the Antarctic continental lithosphere: A review, *Global Planet. Change*, *42*, 155–165. doi:10.1016/j.gloplacha.2003.12.005.

Phillips, G., and A. L. Läufer (2009), Brittle deformation relating to the Carboniferous-Cretaceous evolution of the Lambert Graben, East Antarctica: A precursor for Cenozoic relief development in an intraplate and glaciated region, *Tectonophysics*, *471*, 216–224. doi:10.1016/j.tecto.2009.02.012.

Poupinet, G., and N. M. Shapiro (2009), Worldwide distribution of ages of the continental lithosphere derived from a global seismic tomographic model, *Lithos*, *109*, 125–130. doi:10.1016/j.lithos.2008.10.023.

Reading, A. M. (2006), The seismic structure of Precambrian and early Palaeozoic terranes in the Lambert Glacier region, East Antarctica, *Earth Planet. Sci. Lett.*, *244*, 44–57. doi:10.1016/j.epsl.2006.01.031.

Ritzwoller, M. H., N. M. Shapiro, A. L. Levshin, and G. M. Leahy (2001), Crustal and upper mantle structure beneath Antarctica and surrounding oceans, *J. Geophys. Res.*, *106*(12), 30645–30670.

Roult, G., and D. Rouland (1992), Antarctica I: Deep structure investigations inferred from seismology: A review, *Phys. Earth Planet. Inter.*, *84*, 15–32.

Sambridge, M., and K. Mosegaard (2002), Monte Carlo methods in geophysical inverse problems, *Rev. Geophys.*, *40*(3), 1–29. doi:10.1029/2000GR000089.

Schott, B., and H. Schmeling (1998), Delamination and detachment of a lithospheric rot, *Tectonophysics*, *296*, 225–247.

Sleep, N. H. (2006), Mantle plumes from top to bottom, *Earth Sci. Rev.*, *77*, 231–271. doi:10.1016/j.earscirev.2006.03.007.

Stamps, D. S., E. Calais, E. Saria, C. Hartnady, J.-M. Nocquet, C. J. Ebinger, and R. M. Fernandes (2008), A kinematic model for the East African Rift, *Geophys. Res. Lett.*, *35*, L05304, doi:10.1029/2007GL032781.

Studinger, M., G. D. Karner, R. E. Bell, V. Levin, C. A. Raymond, and A. A. Tikku (2003), Geophysical models for the tectonic framework of the Lake Vostok region, East Antarctica, *Earth Planet. Sci. Lett.*, *216*, 663–677. doi:10.1016/S0012-821X(03)00548-X.

Tingey, R. J. (1991), The regional geology of Archaean and Proterozoic rocks in Antarctica, in *The Geology of Antarctica*, edited by R. J. Tingey, pp. 1–73, Oxford Univ. Press, Oxford, U.K.

van de Flierdt, T., S. R. Hemming, S. L. Goldstein, G. E. Gehrels, and S. E. Cox (2008), Evidence against a young volcanic origin of the Gamburtsev Subglacial Mountains, Antarctica, *Geophys. Res. Lett.*, *35*, L21303, doi:10.1029/2008GL035564.

Veevers, J. J. (1994), Case for the Gamburtsev Subglacial Mountains of East Antarctica originating by mid-Carboniferous shortening of an intracratonic basin, *Geology*, *22*, 593–596.

Veevers, J. J., and A. Saeed (2008), Gamburtsev Subglacial Mountains provenance of Permian-Triassic sandstones in the Prince Charles Mountains and offshore Prydz Bay: Integrated U-Pb and T_{DM} ages and host-rock affinity from detrital zircons, *Gondwana Res.*, *14*, 316–342. doi:10.1016/j.gr.2007.12.007.

Veevers, J. J., A. Saeed, and P. E. O'Brien (2008a), Provenance of the Gamburtsev Subglacial Mountains from U-Pb and Hf analysis of detrital zircons in Cretaceous to Quaternary sediments in Prydz Bay and beneath the Amery Ice Shelf, *Sediment. Geol.*, *211*, 12–32. doi:10.1016/j.sedgeo.2008.08.003.

Veevers, J. J., A. Saeed, N. Pearson, E. Belousova, and P. D. Kinny (2008b), Zircons and clay from morainal Permian siltstone at Mt. Rymill (73°S, 66°E), Prince Charles Mountains, Antarctica, reflect the ancestral Gamburtsev Subglacial Mountains–Vostok Subglacial Highlands complex, *Gondwana Res.*, *14*, 343–354, doi:10.1016/j.gr.2007.12.006.

Visser, K., J. Trampert, and B. L. N. Kennett (2008), Global anisotropic phase velocity maps for higher mode Love and Rayleigh waves, *Geophys. J. Int.*, *172*, 1016–1032. doi:10.1111/j.1365-246X.2007.03685.x.

von Frese, R. R. B., L. Tan, J. W. Kim, and C. R. Bently (1999), Antarctic crustal modeling from the spectral correlation of free-air gravity anomalies with the terrain, *J. Geophys. Res.*, *104*(B11), 25,275–225,296.

Wessel, P., and W. H. F. Smith (1998), New, improved version of Generic Mapping Tools released, *Eos Trans. AGU*, *79*(47).

White, D. J., M. D. Thomas, A. G. Jones, J. Hope, B. Nemeth, and Z. Hajnal (2005), Geophysical transect across a Paleoproterozoic continent-

continent collision zone: The Trans-Hudson Orogen, *Can. J. Earth Sci.*, *42*, 385–402. doi:10.1139/E05-002.

Yang, Y., and D. W. Forsyth (2006), Rayleigh wave phase velocities, small-scale convection, and azimuthal anisotropy beneath southern California, *J. Geophys. Res.*, *111*, B07306, doi:10.1029/2005JB004180.

Yue, H., T. Lay, and K. D. Koper (2012), *En echelon* and orthogonal fault ruptures of the 11 April 2012 great intraplate earthquakes, *Nature*, 490, 245–249, doi:10.1038/nature11492.

Zatman, S., and M. A. Richards (2002), On the evolution of motion across diffuse plate boundaries, in *Plate Boundary Zones*, edited by S. Stein and J. T. Freymueller, pp. 265–281, AGU, Washington, D. C.

Zatman, S., R. G. Gordon, and M. A. Richards (2001), Analytic models for the dynamics of diffuse oceanic plate boundaries, *Geophys. J. Int.*, *145*, 145–156.

Zelt, B. C., and R. M. Ellis (1999), Receiver-function studies in the Trans-Hudson Orogen, Saskatchewan, *Can. J. Earth Sci.*, *36*, 585–603.

Zhao, Y., X. H. Liu, X. C. Liu, and B. Song (2003), Pan-African events in Prydz Bay, East Antarctica, and their implications for East Gondwana tectonics, in *Proterozoic East Gondwana: Supercontinent Assembly and Breakup*, edited by M. Yoshida, B. F. Windley and S. Dasgupta, pp. 231–245, Geol. Soc., London.

Zhou, Y., F. A. Dahlen, and G. Nolet (2004), Three-dimensional sensitivity kernels for the surface-wave observables, *Geophys. J. Int.*, *158*, 142–168. doi:10.1111/j.1365-246X.2004.02324.x.